ACS APPLIED MATERIALS & INTERFACES

Research Article

Cite This: ACS Appl. Mater. Interfaces 2018, 10, 41450−41457

www.acsami.org

Influence of the Magnitude of Ferroelectric Domain Polarization on the Photochemical Reactivity of $BaTiO_3$

Wenjia Song, Paul A. Salvador, and Gregory S. Rohrer*

Department of Materials Science and Engineering, Carnegie Mellon University, Pittsburgh, Pennsylvania 15213, United States

Supporting Information

ABSTRACT: The spontaneous polarization of domains in ferroelectric materials has been used to spatially separate photogenerated electrons and holes, reducing recombination and thereby improving the efficiency of photochemical reactions. Here, the influence of the magnitude of the polarization on photochemical reactivity is investigated. The magnitude of the out-of-plane component of the polarization was characterized by scanning Kelvin probe force microscopy (KFM). By examining crystals with orientations that deviate by only a few degrees from (001), two types of domains were identified: those with polarization vectors nearly perpendicular to the surface and those with polarization vectors nearly parallel to the surface. The photochemical reactivity was measured using topographic atomic force microscopy to determine the amount of Ag^+ (Pb^{2+}) that was photochemically reduced (oxidized) to Ag (PbO_2) on the surface. For the reduction reaction, the reactivities of domains with polarizations nearly perpendicular to the surface were only about 3 times greater than the reactivities of the domains with polarizations nearly parallel to the surface, indicating that, for this reaction, the magnitude of the out-of-plane polarization is less important than its sign. For the oxidation of lead, only the domains with polarizations nearly perpendicular to the surface were reactive, indicating that for this reaction, both the sign and magnitude of the polarization are important.

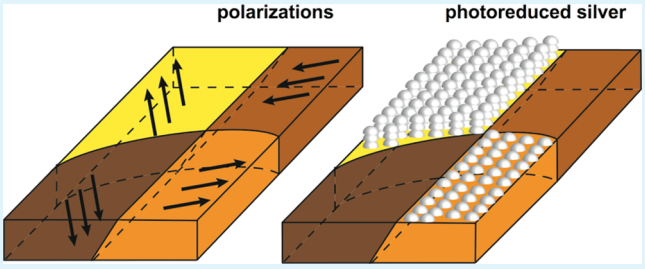

KEYWORDS: *photochemical reactivity, ferroelectric domain, polarization, $BaTiO_3$, atomic force microscopy, Kelvin probe force microscopy*

INTRODUCTION

Ferroelectric metal oxides have been studied extensively for their applications in photochemistry.[1−8] The interest in ferroelectrics stems from the fact that the spontaneous polarization within ferroelectric domains can separate photogenerated electrons and holes and thus minimize the recombination of charge carriers, as well as the back reaction of intermediates. By avoiding losses from recombination, the efficiencies of photochemical reactions can potentially be improved and evidence to support this has been reported.[9−12] Similar observations have been reported for materials in which surface polarization arises from other mechanisms.[13−15] For the design of optimal photocatalysts, it is important to understand how the magnitude of the polarization (or charge) at the surface influences photochemical reactivity yet little is known about this. In the current paper, we experimentally explore the effect of the magnitude of the polarization on photochemical reactivity.

The magnitude of the ferroelectric polarization in the direction perpendicular to the surface is determined by three factors. The first is the intrinsic strength of the polarization determined by the structure itself. For example, the polarization of $BaTiO_3$ is 26 $\mu C/cm^2$ in the [001] direction[16] and the polarization of the $BiFeO_3$ is 6.1 $\mu C/cm^2$ in the [111] direction.[17] The second factor is the size of the depolarization field, which partially compensates the ideal polarization.[3,18] Depolarization fields depend on a number of factors, including the environment.[3] The third factor is the orientation of the polarization axis with respect to the surface of interest. Intuitively, one would expect that a larger magnitude of polarization would lead to improved charge separation and greater photochemical reactivity. Thus, when the polarization axis is perpendicular (parallel) to the surface, it should have the maximum (minimum) effect on the reactivity. To our knowledge, the only systematic studies of such reactivity are calculations by Glickstein et al.,[19] which show that the reactivity increases with the magnitude of the polarization but at a decreasing rate at larger polarizations. Here, we compare the experimental reactivity of $BaTiO_3$ surfaces within a few degrees of the (001) to the orientation of the polarization axis with respect to the surface, which determines the magnitude of the out-of-plane surface polarization.

$BaTiO_3$ is a well-known ferroelectric material and a UV light absorbing, semiconducting photocatalyst.[20] The spontaneous polarization in $BaTiO_3$ is along the [001] direction,[21] and the out-of-plane component of the polarization on the surface

Received: September 28, 2018
Accepted: November 9, 2018
Published: November 9, 2018

DOI: 10.1021/acsami.8b16983
ACS Appl. Mater. Interfaces 2018, 10, 41450−41457

depends on the orientation of the polarization with respect to the surface plane. By using the polished surface of a polycrystalline ceramic, we can access a range of surface orientations within a few degrees of (001) and identify these surface orientations by electron backscatter diffraction (EBSD). The nucleation and the growth of ferroelectric domains are known to depend on the cooling rate.[22−24] Quenching ferroelectrics (including $BaTiO_3$) through the phase transition is known to change the structure of the domains.[25−27] Here, the density of 90 and 180° domain boundaries is controlled via quenching, which thus controls the types of polarization vectors present at the surface.

The purpose of this work is to examine the influence of the magnitude of the polarization on the photochemical reactivity. Crystals with near (001) orientations were located on the surfaces of polycrystalline $BaTiO_3$ samples. Domains with polarizations approximately perpendicular or parallel to the sample surface are readily identified by the distinct shapes of 180 and 90° domain walls. To confirm the variations in the local surface polarization across domains, the surface potential is measured by Kelvin probe force microscopy (KFM).[28] The relative amounts of reaction products on the surfaces of different domains after a fixed time interval are taken as a measure of the relative reactivity.[13] These relative amounts, after the photochemical reduction of silver and oxidation of lead, are measured using atomic force microscopy (AFM).[29−32] The results demonstrate that, for the reduction reaction, a greater polarization leads to a greater photochemical reactivity but that as the magnitude of the polarization increases, the gains in reactivity become smaller. For the lead oxidation reaction, however, products form only on the domains with the greatest negative polarization. These results are consistent with prior calculations of the relationship between the magnitude of the polarization in $BaTiO_3$ and the average surface photocurrents.[19]

EXPERIMENTAL METHODS

Dense polycrystalline $BaTiO_3$ samples were prepared as follows. $BaTiO_3$ powder (99.7%, Alfa Aesar) was mixed with a few drops of PVA as a binder and uniaxially compressed at 570 MPa in a 1 cm diameter cylindrical die (using methanol as a lubricant) to form a pellet with a thickness of ∼2 mm. The pellet was then placed in a covered Al_2O_3 crucible, with some excess $BaTiO_3$ powder at the bottom to reduce potential contamination. Next, the sample was calcined at 900 °C for 10 h to degas, sintered at 1230 °C for 10 h, and finally annealed at 1360 °C for 3 h to grow the grains. All heating processes were carried out in air. A flat and polished surface was achieved through the consecutive use of 600, 800, and 1200 grit silicon carbide abrasive papers (Buehler) and 9, 3, 1, and 0.05 μm diamond suspensions (Buehler). The specimen was then thinned to ∼800 μm by grinding the opposite side. We found that the surface potential measurement worked better on thinner samples, presumably because of the lower through-thickness resistance. The sample was loaded with a force of ∼450 g during the grinding and the polishing process. The polished sample was then wiped with cotton swabs and ultrasonically cleaned in water. Finally, the sample was annealed at 1225 °C for 4 h to repair polishing damage and thermally etch the grain boundaries; it was cooled at 5 °C/min. Visible light microscopy indicated that the grain size was in the range of 10−100 μm. Some of the samples were then heated to 200 °C, well above the 120 °C Curie temperature of $BaTiO_3$,[33] and subsequently quenched in deionized (DI) water at room temperature. Quenching increases the density of 180° domain boundaries, but the domain structure of the quenched sample evolves with time, ultimately reducing the density of 180° domain boundaries.[34] Thus, experiments must be carried out soon after quenching.

Electron backscatter diffraction was used to measure the orientations of the crystals at the surface of the $BaTiO_3$ ceramic. The diffraction patterns were acquired using a Quanta 200 (FEI) scanning electron microscope (SEM) system. Typical microscope parameters were as follows: 70° for the angle between the electron beam and the sample surface, 20 kV for the accelerating voltage, 5.0 nm for the spot size, and 10 mm for the working distance. The same system was also used in secondary electron (SE) scanning mode, with similar parameters except for the angle being 0°. EBSD patterns were recorded with a step size of ∼1 μm. A description of the EBSD data processing can be found in the Supporting Information.

Photochemical marker reactions were used to measure the photochemical reactivity, as described previously.[29−32] The photoreduction of silver ($Ag^+(aq) \rightarrow Ag(s)$) and the photooxidation of lead ($Pb^{2+}(aq) \rightarrow PbO_2(s)$) deposit insoluble products on the surfaces that mark the reaction locations; the amounts of each product phase indicate the relative photochemical reactivity.[35−37] An O-ring was placed on top of the sample, and a few drops of 0.115 M $AgNO_3$ (Acros) or $Pb(CH_3COO)_2$ (MilliporeSigma) aqueous solution were added to fill the volume enclosed by the O-ring. A quartz slip was then placed on top to seal the system by capillarity and provide a uniform exposure surface. Afterward, the whole assembly was illuminated by a mercury lamp (Newport) operated at 300 W for 7 s for silver reduction and 180 s for lead oxidation. Skin and eyes must be protected to prevent damage from UV radiation during the illumination. After the reaction, the quartz slip and the O-ring were removed and the sample was rinsed in DI water to remove the excess salts. The sample was then dried with compressed air. Note that the order of the reactions appears to influence the reactivity for the photooxidation of lead. If the sample is first used to photoreduce silver, cleaned, and then used to photooxidize lead, the rate of the oxidation reaction is greater than if a fresh surface is used. This is presumably because of residual silver (not visible in SEM or AFM images) that contaminates the surface and promotes the reaction.

The surface topography after the photochemical reactions was characterized by AFM using an NTEGRA (NT-MDT) microscope operated in semicontact mode. The Gwyddion software package[38] was employed to process and analyze the data. All topographic AFM images were leveled using the "median level" and "remove arc" operations to create a flat baseline before extracting the profiles. After each reaction, the surface was wiped with cotton swabs and cleaned ultrasonically. The surface was observed again under AFM to ensure that there were no observable reaction products. The same microscope was then used to map the surface potential by KFM in noncontact mode. Pt/Ir-coated conductive probes were used for KFM and a voltage of 6.5 V was applied while scanning. The KFM images were also processed using Gwyddion software package.[38]

RESULTS

The EBSD data were used to identify grains with surface orientations near (001); examples can be found in Figure S1. A topographic AFM image of the surface after the photochemical reduction of silver is shown in Figure 1a,b for the sample that was slow-cooled (quenched). The orientations of the surfaces in Figure 1a,b were both measured to be less than 5° from the (001) orientation. The bright striped contrast in the AFM images corresponds to the reduced metallic silver. The darkest contrast arises from polishing scratches and grain boundaries. Ninety degree domain walls have {110} orientations,[39] and they intercept the surfaces along straight lines, as observed in both AFM images. The "ladderlike" patterns arise from typical arrangements of two different 90° domain walls; this feature is characteristic of (001) oriented surfaces. One hundred and eighty degree domain walls can take any orientation in the [001] zone, are curved, and form closed loops on the (001) surface. These boundaries are most obvious on the surface of the quenched sample in Figure 1b.

DOI: 10.1021/acsami.8b16983
ACS Appl. Mater. Interfaces 2018, 10, 41450−41457

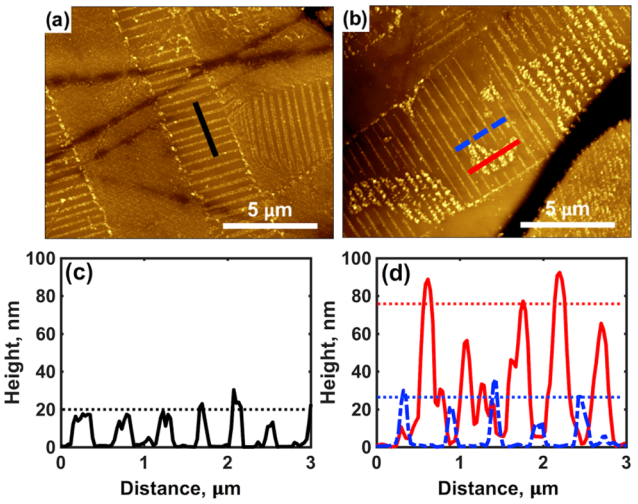

Figure 1. (a, b) Topographic AFM images on a $BaTiO_3$ surface with an orientation close to (001) after a photochemical reaction in aqueous silver nitrate solution. The sample was annealed and (a) cooled at the rate of 5 °C/min in air (b) quenched in DI water at room temperature. The topographic contrast in both images is 140 nm from black to white. (c, d) The height profiles along the lines in (a) and (b). The horizontal dotted lines show the average height of the deposits.

The heights of the photochemically reduced silver deposits are used as a measure of the photochemical reactivity for reduction. We focus here on the reactivity in the areas within the ladders (we will comment briefly on the reactivity in the areas between the ladders in the Discussion section). In the slowly cooled sample shown in Figure 1a, there is primarily one level of reactivity for the area inside the ladder. But for the quenched sample shown in Figure 1b, there are two levels of reactivity for the area inside the ladder. The height profiles in Figure 1c,d are consistent with that qualitative observation. The horizontal dotted lines indicate the average of the maximum heights of each silver stripe. For the quenched sample, the height of the silver deposit on the more reactive domain (red lines) is about 3 times larger than that on both the less reactive domain in the quenched sample (blue lines) and the reactive domains in the slowly cooled sample (black lines). Note, a similar domain pattern was observed previously using the conventional etching technique.[40]

KFM was used to probe the surface potentials of the ferroelectric domains that have different levels of photochemical reactivity for the reduction of silver. Representative topographic AFM images and the associated KFM images of both the slowly cooled and the quenched samples are shown in Figure 2. These two grains are 6° from the (001) orientation (see Figure S1 for details). Some of the dark contrast in the topographic AFM images correlates to scratches and pits on the $BaTiO_3$ surface. Note that these features have only a minor influence on the contrast in the surface potential images. The KFM image in Figure 2b appears to have two levels of surface potential in a striped pattern, and the image in Figure 2e appears to have four levels of surface potential, with stripes superimposed on regions separated by curved lines. To obtain average values for these different contrast levels, rectangular boxes were drawn on the KFM images, as marked in Figure 2b,e, so that each box includes ~300 data points. The average value and the standard deviation of the points within each box were calculated and are plotted as a function of location, where each location is denoted by a capital letter, A−F. The profiles in Figure 2c,f confirm that two levels of surface potential are observed on the slowly cooled sample, whereas four levels of surface potential are observed on the quenched sample. In addition, note that in Figure 2e, continuous, straight, vertically

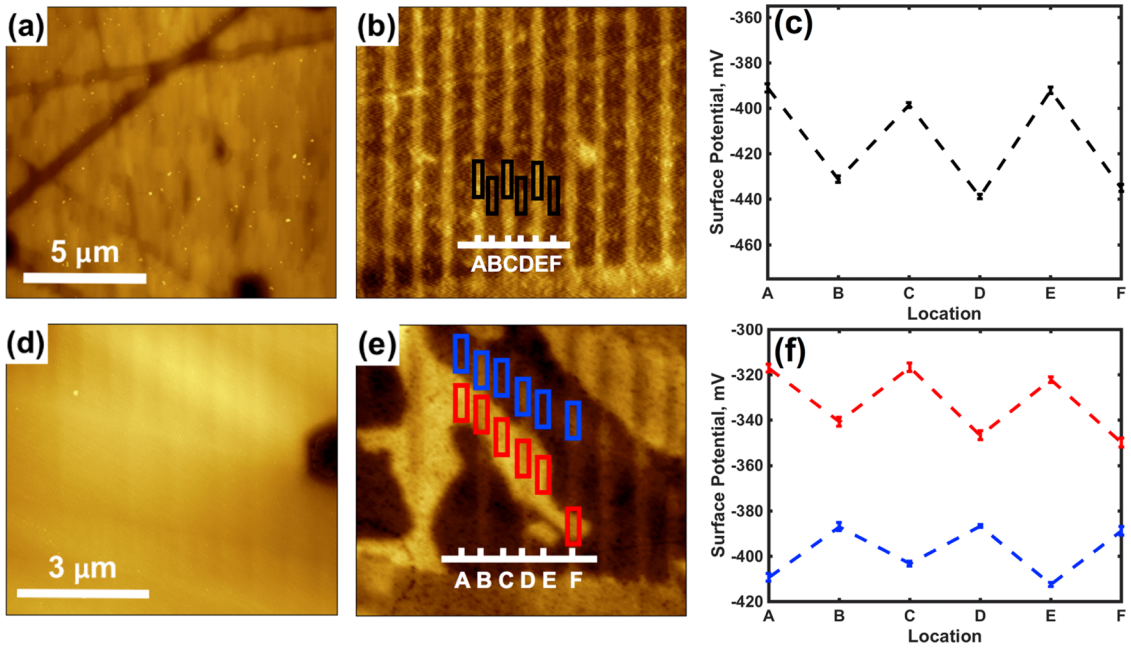

Figure 2. (a, d) Topographic AFM images and the associated (b, e) surface potential images. (a) and (b) are within the (L) grain region, as indicated in Figure S1; this $BaTiO_3$ sample was cooled at the rate of 5 °C/min in air. (d) and (e) are from the (R) grain region identified in Figure S1; this $BaTiO_3$ sample was quenched in DI water at room temperature. The black-to-white contrast is (a) 150 nm, (b) 140 mV, (d) 90 nm, and (e) 190 mV. (c, f) The average surface potential and standard deviation calculated from the data points within the box marked by the same letter and the same color in (b) and (e). The lines are added to guide the eye.

DOI: 10.1021/acsami.8b16983
ACS Appl. Mater. Interfaces 2018, 10, 41450−41457

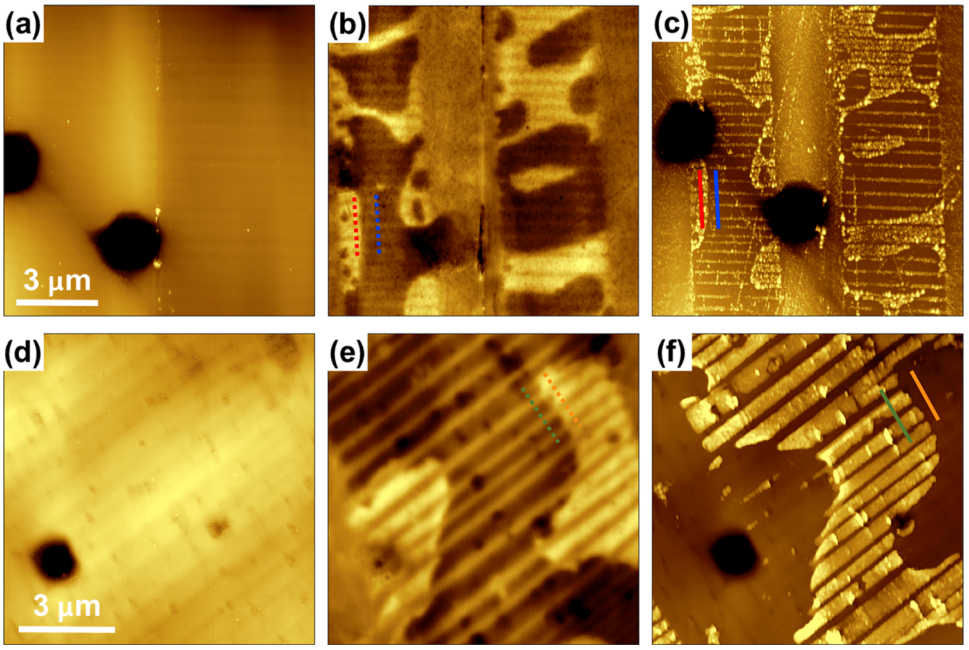

Figure 3. (a) Topographic AFM image, (b) surface potential image, and (c) topographic AFM image after silver reduction. The images are from the same area of the surface on the grain marked "L" in Figure S1. (d) Topographic AFM image, (e) surface potential image, and (f) topographic AFM image after a photochemical reaction in a lead acetate solution. The images are from the same area of the surface on the grain marked "R" in Figure S1. The black-to-white vertical scales are (a) 90 nm, (b) 220 mV, (c) 110 nm, (d) 63 nm, (e) 220 mV, and (f) 85 nm. The sample was quenched in room temperature DI water.

aligned 90° domains are interrupted by a curved, diagonal 180° domain wall and that the relative potentials on either side of the 180° wall are inverted. In other words, the brighter of the two 90° domains below the 180° boundary changes to the darker of the two domains above the boundary. This is also evident from the average potentials in Figure 2f. It is noted that the absolute surface potential measurements in KFM images can vary with the instrument setup and the KFM probe itself, so we focus on the relative values of the potentials within Figure 2b,e rather than the specific values of the potentials.

Figure 3a–c shows a topographic AFM image, the corresponding KFM image, and a topographic AFM image after silver photoreduction of the same area on a quenched $BaTiO_3$ sample; the field of view is within the grain labeled "L" in Figure S1. The two darkest regions on both topography images arise from two surface pits. The domain pattern in the surface potential map, Figure 3b, matches the silver deposition pattern in Figure 3c. Consistent with the data in Figure 2, four levels of surface potential and two levels of photocathodic reactivity can be identified in Figure 3b,c, respectively. Figure 3d–f compares a topographic AFM image, the corresponding KFM image, and a topographic AFM image at the same location on the surface inside grain "R" (as labeled in Figure S1) after illumination in an aqueous lead acetate solution. The dark circle at the bottom left corner in the topographic images arises from a surface pit. Some of the 90° domain walls visible in the KFM map can also be identified in Figure 3d. The reaction product appears as a bright even coating, as shown in Figure 3f. Compared to Figure 3c, the oxidation product is found on the domains with the lowest potential instead of those with the higher potential; these are the photoanodic domains. Furthermore, only a single level of oxidation reactivity is apparent in Figure 3f, compared with the two levels of reduction activity. It is not clear why there are not two different photoanodic areas on the surface with different reactivities (parallel to the two photocathodic areas). However, this might be related to the fact that the oxidation reaction is more complex than the reduction reaction. The photoanodic reaction requires four charge carriers compared with one, is mediated by hydroxyl radicals,[37] and is driven by minority carriers. Another possible reason that the photoanodic reaction is weaker than the photocathodic reaction is the different driving forces. In both cases, the overall reactivity is limited by the slower of the two half reactions. For the photocathodic reaction, this is the oxidation of water, and for the photoanodic reaction, it is the oxidation of Pb^{2+}. The lead oxidation level of 1.46 V/normal hydrogen electrode (NHE),[41] compared to the water oxidation level of 1.23 V/NHE,[41] is closer to the valence band edge of $BaTiO_3$ (~3.2 V/NHE)[42] and thus provides a smaller driving force for the oxidation reaction. Although a variety of reaction times were explored, only a single level of reactivity was observed.

Figure 4 shows topographic and surface potential profiles extracted from the images in Figure 3b,c,e,f along the lines drawn on the images. Each panel compares the profiles along parallel lines separated by a 180° domain boundary. Comparing the upper and lower panels makes it possible to correlate the heights of the reaction products with the changes in the surface potential. The horizontal dotted lines in Figure 4b,d indicate the average height at the maximum positions over each deposit. When the curves are compared within panels (a)–(c), it is clear that the 180° boundary inverts the surface potential and the reactivity. For example, in panels (a) and (c), the positions where the red (orange) line reaches a peak (valley) are approximately the positions where the blue (green) line reaches a valley (peak). Moreover, the maxima of the solid lines (Figure 4b,d) approximately match the maxima of the dotted lines (Figure 4a,c) of the same color.

DOI: 10.1021/acsami.8b16983
ACS Appl. Mater. Interfaces 2018, 10, 41450–41457

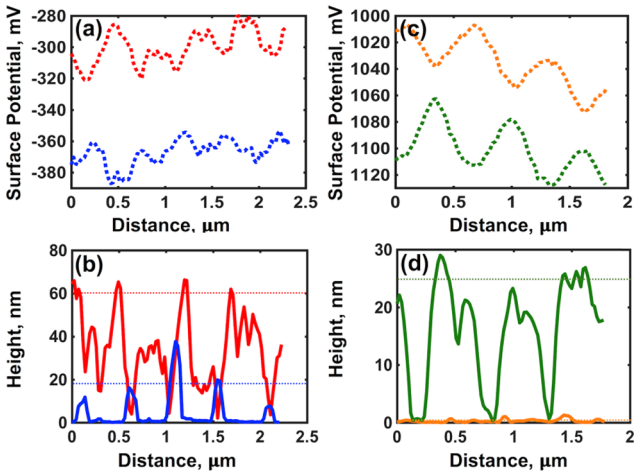

Figure 4. (a, c) Comparison of the surface potential corresponding to the traces of the same color in Figure 3b,e. (b, d) Comparison of the silver deposition height and the lead-containing product deposition height along the traces of the same color in Figure 3c,f, respectively. The horizontal dotted line shows the average deposition height.

This is consistent with the images in Figure 3b,c,e,f, which show that the surface potential map and the marker reaction product height are correlated. We note that the correlation between the surface potential and the heights of the silver deposits in Figure 4 is not perfect. The main reason for this is that the domain structure of the quenched sample evolves with time, ultimately reducing the density of 180° domains.[34] This phenomenon is illustrated by the images in Figure S2. The domain structure produced by quenching is not stable at room temperature; the 180° domain walls are higher in energy than the 90° domain walls[43] and during several days of aging at room temperature are mostly eliminated from the microstructure. Consistent with the results shown in Figure 1d, the heights of the silver on the more reactive domain, as indicated by the red solid line in Figure 4b, are about 3 times greater than on the less reactive domain, as shown by the blue solid line in Figure 4b.

DISCUSSION

In this study, we have found four distinguishable levels of surface potential on the surfaces of quenched $BaTiO_3$ grains with near-(001) orientations (see Figure 2f). The four potential levels were correlated to two areas of photocathodic reactivity (see Figure 1d), one area of photoanodic reactivity and one inert area. Using what is known about the domain structure of $BaTiO_3$, it is possible to construct a model for the microstructure that explains these observations. To do so, a surface potential map, recorded from the grain marked "R" in Figure S1 that is 6.3° from [001], is shown in Figure 5a. The topographic AFM image recorded after the silver reduction reaction on the same area of grain R, is given in Figure 5d. In both images, the boundaries between four representative domains have been marked with black lines and the domains have been labeled with numbers. To construct the model, four assumptions are made. First, the spontaneous polarization is along [001] in $BaTiO_3$.[21] Second, straight domain walls at the surface arise from the intersections with the surface of 90° domain walls, which are twin planes with {110} orientations.[39] Third, 90° domain walls are charge neutral, which means that the two polarizations on either side should follow a head-to-tail pattern. Fourth, 90° domain walls separate polarizations that are perpendicular to each other, whereas the 180° domain walls separate polarizations that are antiparallel to each other. Note that the observed curvature of the 180° domain walls (see Figure 5a) implies that these boundaries have some charge when they are not parallel to the polarization.

Recalling that the photocathodic domains that reduce silver have been shown to be positive domains where the polarization points toward the surface,[32] domains 1 and 2 can be assigned as positive domains. Because domain 1 is more reactive, it can be assigned as having a larger polarization magnitude. Thus, we assign domain 1 as having a positive polarization nearly perpendicular to the surface (rotated by about 6° from the surface normal). The assignment of the remaining domains follows from the assumptions listed above. Domains 1 and 4 (and 2 and 3) are separated by a 180° boundary and are thus antiparallel to each other. Domains 1 and 3 (and 4 and 2) are separated by a 90° boundary, which

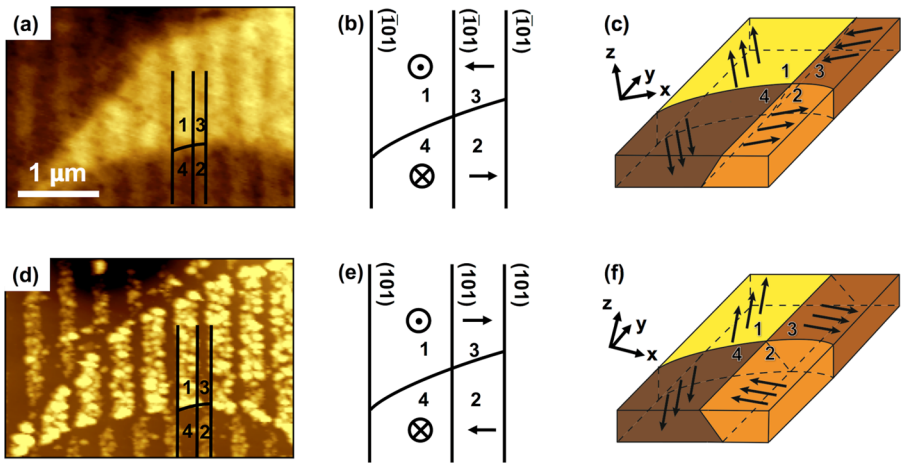

Figure 5. (a) Surface potential image and (d) topographic AFM image after the photochemical reduction of silver of the same area within the (R) grain region, as marked in Figure S1. The black-to-white contrast is 160 mV in (a) and 70 nm in (d). (b, e) Schematics showing the two possible polarizations and the corresponding domain wall orientations on a (001) grain surface. (c, f) Three-dimensional schematics indicating the two possible cases on a grain close to (001). The crystallographic coordinate system was slightly rotated in opposite directions, as shown by the insets in (c) and (f).

DOI: 10.1021/acsami.8b16983
ACS Appl. Mater. Interfaces 2018, 10, 41450−41457

leads to two potential scenarios for domain orientations. If the surface was in the exact (001) orientation, where the polarization in domain 1 would be perpendicular to the surface, the two cases are shown in Figure 5b,e. These schematics are shown for simplicity. Schematics for the real surface, where the orientation is rotated from (001) by about 6°, are shown as oblique projections in Figure 5c,f.

The surface reactivity now follows naturally from the schematics in Figure 5c,f. Domain 1 has the largest positive out-of-plane polarization magnitude. Domains of this sort have the highest surface potential and reduce the most silver, as shown in Figure 5a,d. Conversely, domain 4 has the largest negative out-of-plane polarization magnitude. Domains of this sort have the lowest surface potential and are photoanodic (oxidize lead), as shown in Figure 3e,f. Because of the slight rotation from the (001) orientation, domain 2 has a small positive out-of-plane polarization component, whereas domain 3 has a small negative out-of-plane polarization component. These small out-of-plane polarizations are apparently strong enough to influence reactivity; domains with polarizations similar to domain 3 suppress reduction, whereas domains with polarizations similar to domain 2 promote reduction. Apparently, the weak negative polarization of domain 3 did not promote a second (weaker) level of reactivity for lead oxidation but that observation does not contradict the model for the domain orientation, surface potential, and reactivity.

While the schematics in Figure 5 account well for the results, there is one significant difference: the surface potential in domain 3 should be lower than that in domain 2, but this is not the case in the image (Figure 5a). Similar results were obtained for the domains shown in Figures 2 and 3 (in fact it was a general observation). We believe that this is a result of the microscope's resolution, resulting in a convolution signal from adjacent domains. The widths of the domains in Figure 5a,d are only about 250 nm. When the tip measures the potential, it is above the surface and affected by the electric field of the neighboring domains. When the tip is over domain 3 (or domain 2), the KFM measures a reduction (an increase) in the local potential compared with domain 1 (domain 4) but actual values in any domain are convolutions of the potentials from adjacent domains. Thus, the strong out-of-plane component dominates the measured value in these 90° domain ladders, consistent with the observations.

As noted in the description of Figure 1, irregular contrast from small amounts of reduced silver is sometimes observed in the areas between the ladders. A striped pattern of silver is sometimes visible and when it is, the angle at which the stripes meet is 45°. (The left bottom part of Figure 1a is enlarged and shown in Figure S3.) In other cases, the entire area is unreactive or weakly reactive. These observations are consistent with the model proposed above. These regions are thought to have 90° domain boundaries, with the polarization vectors nearly in the surface plane, as illustrated schematically in Figure S4. In these cases, however, their out-of-plane polarization is sensitive to the exact misalignment of the [001] axis. In this case, alternating domains can have both small positive out-of-plane components and small negative out-of-plane components or small positive and negative out-of-plane components can alternate. Thus, the contrast is weak and variable, depending on the exact misorientation from [001].

The most interesting result from this work is that two sets of domains with different magnitudes of the out-of-plane polarization were induced by quenching $BaTiO_3$; one set of domains with out-of-plane polarizations almost perpendicular to the surface and the other set of domains with nearly in-plane polarizations. The photocathodic reactivity of domain 1, where the positive polarization is almost perpendicular to the surface and the out-of-plane polarization is 0.99 P_{BTO} (full polarization P_{BTO} = 26 $\mu C/cm^2$ for $BaTiO_3$ at room temperature[44]), is only about 3 times greater than the photocathodic reactivity of domain 2, whose positive out-of-plane component of the polarization is only 1/10th of that in domain 1 ($\sin 6° \approx 0.1$ P_{BTO}). This is consistent with recent simulation results, where the surface average hole current (related to the photochemical reactivity) was correlated to the magnitude of the polarization in multidomain $BaTiO_3$ coated with thin TiO_2 films.[19] The simulation results are plotted in Figure 6, with data points

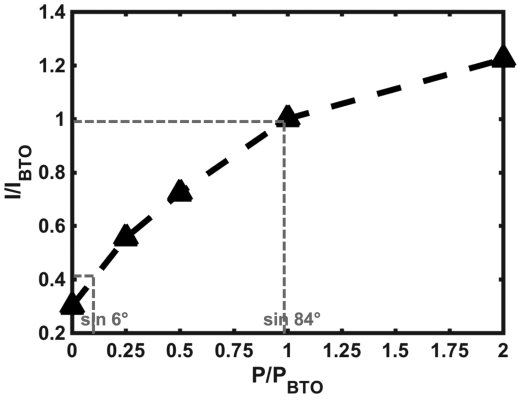

Figure 6. Simulated dependence of the relative surface average hole current on polarization magnitude, plotted using the simulation results from ref 19. The gray vertical lines at sin 6° and sin 84° correspond to domains 2 and 1 in Figure 5. The lines are added to guide the eye.

marked by triangles (and a dashed line to guide the eye). It should be mentioned that the relative current, I, on the vertical axis (or relative polarization, P, on the horizontal axis) is normalized by the current, I_{BTO}, (or polarization P_{BTO}) at full polarization. Thus, at full polarization, the relative values of current and polarization are 1 on this graph. The two sets of vertical gray lines denote the location of sin 6° and sin 84°, which correspond to the relative polarization values, respectively, of domains 2 and 1 in Figure 5. It is clear that the photochemical reactivity, indicated by the relative current values at the horizontal gray lines, only increases by a factor of 2−3 when the magnitude of the polarization changes by a factor of 10. In all of the topographic AFM images where two levels of reactivity were observed for grains near the (001), the relative heights of the silver deposits were approximately 3−1, consistent with the results of the simulation.

There have been numerous previous studies of the photochemical reactivity of ferroelectric materials using marker reactions.[31,32,45−49] The consistent conclusion has always been that the product of the photoreduction reaction forms on positive domains, where a positive component of the polarization vector is directed toward the surface, whereas the photooxidation product forms on spatially complementary and oppositely charged domains, where the polarization has a component directed into the bulk. The observations discussed here are consistent with this prior interpretation. What is surprising is that even domains with a very small positive out-of-plane component, only 1/10 P_{BTO} or ≈2−3 $\mu C/cm^2$, are

DOI: 10.1021/acsami.8b16983
ACS Appl. Mater. Interfaces 2018, 10, 41450−41457

photocathodically activated. Moreover, our results support the simulated results that indicate increasing the magnitude of the out-of-plane component by a factor of 10 only increases the reactivity by a factor of 3. This suggests that the sign of the polarization is more important than the magnitude. A previous study of $BiFeO_3$ led to the same conclusion, but this was attributed to the material's properties, where the space charge region in $BiFeO_3$ is much larger than the penetration depth of the light.[45] For $BaTiO_3$, this possibility can be excluded, because the adsorption depth is estimated to be much larger than the space charge region width.[42] In contrast, a small negative component of polarization is insufficient to promote the photooxidation reaction, at least when it occurs on the same surface as domains with a strong negative polarization. Prior research on surfaces with random orientations suggests that the negative polarization does not have to be oriented very close to the normal direction to be active for oxidation.[49] However, for the near (001) surfaces studied here, the only photoanodic domains are those whose polarizations are directed almost directly into the bulk.

The findings of the present study have important implications in the design of ferroelectric photocatalysts, as well as other photocatalysts that use surface charge to modify internal fields. Our results confirm that significant modifications in local surface reactivity occur on surfaces with relatively modest out-of-plane polarizations (or surface charge). This indicates there are design opportunities in materials with near-surface internal electric fields generated by other mechanisms, most of which are generally thought to have smaller polarization values than ferroelectricity, including polar surface terminations,[13] flexoelectric effects,[14,15] and heterojunctions between phases with different Fermi levels.[50]

CONCLUSIONS

Domains with different polarizations were induced in $BaTiO_3$ grains with surface orientations close to (100) by quenching polycrystalline ceramics. The multilevel domain structure led to multilevel surface charge states (measured by KFM) and multilevel photochemical reactivity. For the photoanodic oxidation of lead, only those domains with negative polarizations close to the surface normal were reactive, indicating a strong out-of-plane polarization is required. However, the photocathodic deposition of Ag on domains with positive polarizations 6° from the surface normal was only 3 times as great as that on domains with positive polarizations 84° from the sample normal, despite the 10-fold difference in out-of-plane polarization. These results indicate that the photocathodic reactivity increases with the magnitude of the ferroelectric polarization but the influence of the magnitude of the polarization on photochemical reactivity is diminished as the polarization increases.

ASSOCIATED CONTENT

Supporting Information

The Supporting Information is available free of charge on the ACS Publications website at DOI: 10.1021/acsami.8b16983.

EBSD data processing method; EBSD map of the polycrystalline $BaTiO_3$ surface; secondary electron images on a quenched $BaTiO_3$ surface after silver photoreduction showing the domain structure evolution over time; an enlarged image of the left bottom part of Figure 1a; schematics to explain the possible 45° stripes of weak reactivity between the ladders in Figure 1a (PDF)

AUTHOR INFORMATION

Corresponding Author

*E-mail: gr20@andrew.cmu.edu.

ORCID

Wenjia Song: 0000-0002-7628-2900
Paul A. Salvador: 0000-0001-7106-0017
Gregory S. Rohrer: 0000-0002-9671-3034

Notes

The authors declare no competing financial interest.

ACKNOWLEDGMENTS

The authors acknowledge the support of National Science Foundation grant DMR 1609369 and use of the Materials Characterization Facility at Carnegie Mellon University supported by grant MCF-677785.

REFERENCES

(1) Tiwari, D.; Dunn, S. Photochemistry on a Polarisable Semiconductor: What Do We Understand Today? *J. Mater. Sci.* **2009**, *44*, 5063−5079.

(2) Li, L.; Salvador, P. A.; Rohrer, G. S. Photocatalysts with Internal Electric Fields. *Nanoscale* **2014**, *6*, 24−42.

(3) Kakekhani, A.; Ismail-Beigi, S.; Altman, E. I. Ferroelectrics: A Pathway to Switchable Surface Chemistry and Catalysis. *Surf. Sci.* **2016**, *650*, 302−316.

(4) Khan, M. A.; Nadeem, M. A.; Idriss, H. Ferroelectric Polarization Effect on Surface Chemistry and Photo-Catalytic Activity: A Review. *Surf. Sci. Rep.* **2016**, *71*, 1−31.

(5) Lou, Z.; Wang, P.; Huang, B.; Dai, Y.; Qin, X.; Zhang, X.; Wang, Z.; Liu, Y. Enhancing Charge Separation in Photocatalysts with Internal Polar Electric Fields. *ChemPhotoChem* **2017**, *1*, 136−147.

(6) Batzill, M. Fundamental Aspects of Surface Engineering of Transition Metal Oxide Photocatalysts. *Energy Environ. Sci.* **2011**, *4*, 3275−3286.

(7) Kalinin, S. V.; Morozovska, A. N.; Chen, L. Q.; Rodriguez, B. J. Local Polarization Dynamics in Ferroelectric Materials. *Rep. Prog. Phys.* **2010**, *73*, No. 056502.

(8) Gruverman, A.; Kholkin, A. Nanoscale Ferroelectrics: Processing, Characterization and Future Trends. *Rep. Prog. Phys.* **2006**, *69*, 2443−2474.

(9) Inoue, Y.; Sato, K.; Sato, K.; Miyama, H. Photoassisted Water Decomposition by Ferroelectric Lead Zirconate Titanate Ceramics with Anomalous Photovoltaic Effects. *J. Phys. Chem.* **1986**, *90*, 2809−2810.

(10) Liu, X.; Kitamura, K.; Terabe, K.; Hatano, H.; Ohashi, N. Photocatalytic Nanoparticle Deposition on $LiNbO_3$ Nanodomain Patterns via Photovoltaic Effect. *Appl. Phys. Lett.* **2007**, *91*, No. 044101.

(11) Li, L.; Rohrer, G. S.; Salvador, P. A. Heterostructured Ceramic Powders for Photocatalytic Hydrogen Production: Nanostructured TiO_2 Shells Surrounding Microcrystalline $(Ba,Sr)TiO_3$ Cores. *J. Am. Ceram. Soc.* **2012**, *95*, 1414−1420.

(12) Munprom, R.; Salvador, P. A.; Rohrer, G. S. Ferroelastic Domains Improve Photochemical Reactivity: A Comparative Study of Monoclinic and Tetragonal $(Bi_{1-0.5x}Na_{0.5x})(V_{1-x}Mo_x)O_4$ Ceramics. *J. Mater. Chem. A* **2016**, *4*, 2951−2959.

(13) Giocondi, J. L.; Rohrer, G. S. Structure Sensitivity of Photochemical Oxidation and Reduction Reactions on $SrTiO_3$ Surfaces. *J. Am. Ceram. Soc.* **2003**, *86*, 1182−1189.

(14) Munprom, R.; Salvador, P. A.; Rohrer, G. S. Polar Domains at the Surface of Centrosymmetric $BiVO_4$. *Chem. Mater.* **2014**, *26*, 2774−2776.

DOI: 10.1021/acsami.8b16983
ACS Appl. Mater. Interfaces 2018, 10, 41450−41457

(15) Pisat, A. S.; Rohrer, G. S.; Salvador, P. A. Spatial Selectivity of Photodeposition Reactions on Polar Surfaces of Centrosymmetric Ferroelastic γ-WO_3. *J. Mater. Chem. A* **2017**, *5*, 8261−8266.
(16) Lines, M. E.; Glass, A. M. *Principles and Applications of Ferroelectrics and Related Materials*; Clarendon Press: Oxford, 1977.
(17) Teague, J. R.; Gerson, R.; James, W. J. Dielectric Hysteresis in Single Crystal $BiFeO_3$. *Solid State Commun.* **1970**, *8*, 1073−1074.
(18) Frey, M. H.; Payne, D. A. Grain-Size Effect on Structure and Phase Transformations for Barium Titanate. *Phys. Rev. B* **1996**, *54*, 3158−3168.
(19) Glickstein, J. J.; Salvador, P. A.; Rohrer, G. S. Multidomain Simulations of Coated Ferroelectrics Exhibiting Spatially Selective Photocatalytic Activity with High Internal Quantum Efficiencies. *J. Mater. Chem. A* **2016**, *4*, 16085−16093.
(20) Casella, R. C.; Keller, S. P. Polarized Light Transmission of $BaTiO_3$ Single Crystals. *Phys. Rev.* **1959**, *116*, 1469−1473.
(21) Kay, H. F. H. F.; Vousden, P. XCV. Symmetry Changes in Barium Titanate at Low Temperatures and Their Relation to Its Ferroelectric Properties. *London, Edinburgh, Dublin Philos. Mag. J. Sci.* **1949**, *40*, 1019−1040.
(22) Alberici-Kious, F.; Bouchaud, J. P.; Cugliandolo, L. F.; Doussineau, P.; Levelut, A. Aging in $K_{1-x}Li_xTaO_3$: A Domain Growth Interpretation. *Phys. Rev. Lett.* **1998**, *81*, 4987−4990.
(23) Likodimos, V.; Orlik, X. K.; Pardi, L.; Labardi, M.; Allegrini, M. Dynamical Studies of the Ferroelectric Domain Structure in Triglycine Sulfate by Voltage-Modulated Scanning Force Microscopy. *J. Appl. Phys.* **2000**, *87*, 443−451.
(24) Inagaki, Y.; Kakimoto, K.; Kagomiya, I. Ferroelectric Domain Characterization of Orthorhombic Sodium-Potassium Niobate Piezoelectric Crystals. *J. Am. Ceram. Soc.* **2010**, *93*, 4061−4065.
(25) Fousek, J.; Šafránková, M. On the Equilibrium Domain Structure of $BaTiO_3$. *Jpn. J. Appl. Phys.* **1965**, *4*, 403−408.
(26) Choi, T.; Horibe, Y.; Yi, H. T.; Choi, Y. J.; Wu, W.; Cheong, S.-W. Insulating Interlocked Ferroelectric and Structural Antiphase Domain Walls in Multiferroic $YMnO_3$. *Nat. Mater.* **2010**, *9*, 253−258.
(27) Chae, S. C.; Lee, N.; Horibe, Y.; Tanimura, M.; Mori, S.; Gao, B.; Carr, S.; Cheong, S.-W. Direct Observation of the Proliferation of Ferroelectric Loop Domains and Vortex-Antivortex Pairs. *Phys. Rev. Lett.* **2012**, *108*, No. 167603.
(28) Vatel, O.; Tanimoto, M. Kelvin Probe Force Microscopy for Potential Distribution Measurement of Semiconductor Devices. *J. Appl. Phys.* **1995**, *77*, 2358−2362.
(29) Fleischauer, P. D.; Alan Kan, H. K.; Shepherd, J. R. Quantum Yields of Silver Ion Reduction on Titanium Dioxide and Zinc Oxide Single Crystals. *J. Am. Chem. Soc.* **1972**, *94*, 283−285.
(30) Morris Hotsenpiller, P. A.; Bolt, J. D.; Farneth, W. E.; Lowekamp, J. B.; Rohrer, G. S. Orientation Dependence of Photochemical Reactions on TiO_2 Surfaces. *J. Phys. Chem. B* **1998**, *102*, 3216−3226.
(31) Giocondi, J. L.; Rohrer, G. S. Spatially Selective Photochemical Reduction of Silver on the Surface of Ferroelectric Barium Titanate. *Chem. Mater.* **2001**, *13*, 241−242.
(32) Giocondi, J. L.; Rohrer, G. S. Spatial Separation of Photochemical Oxidation and Reduction Reactions on the Surface of Ferroelectric $BaTiO_3$. *J. Phys. Chem. B* **2001**, *105*, 8275−8277.
(33) Merz, W. J. The Effect of Hydrostatic Pressure on the Curie Point of Barium Titanate Single Crystals. *Phys. Rev.* **1950**, *78*, 52−54.
(34) Bradt, R. C.; Ansell, G. S. Aging in Tetragonal Ferroelectric Barium Titanate. *J. Am. Ceram. Soc.* **1969**, *52*, 192−198.
(35) Tanaka, K.; Harada, K.; Murata, S. Photocatalytic Deposition of Metal Ions onto TiO_2 Powder. *Sol. Energy* **1986**, *36*, 159−161.
(36) Herrmann, J.-M.; Disdier, J.; Pichat, P. Photocatalytic Deposition of Silver on Powder Titania: Consequences for the Recovery of Silver. *J. Catal.* **1988**, *113*, 72−81.
(37) Torres, J.; Cervera-March, S. Kinetics of the Photoassisted Catalytic Oxidation of Pb(II) in TiO_2 Suspensions. *Chem. Eng. Sci.* **1992**, *47*, 3857−3862.
(38) Nečas, D.; Klapetek, P. Gwyddion: An Open-Source Software for SPM Data Analysis. *Cent. Eur. J. Phys.* **2012**, *10*, 181−188.
(39) Little, E. A. Dynamic Behavior of Domain Walls in Barium Titanate. *Phys. Rev.* **1955**, *98*, 978−984.
(40) Arlt, G.; Sasko, P. Domain Configuration and Equilibrium Size of Domains in $BaTiO_3$ Ceramics. *J. Appl. Phys.* **1980**, *51*, 4956−4960.
(41) Bard, A. J.; Faulkner, L. R.; Leddy, J.; Zoski, C. G. *Electrochemical Methods: Fundamentals and Applications*; Wiley: New York, 1980.
(42) Bhardwaj, A.; Burbure, N. V.; Gamalski, A.; Rohrer, G. S. Composition Dependence of the Photochemical Reduction of Ag by $Ba_{1-x}Sr_xTiO_3$. *Chem. Mater.* **2010**, *22*, 3527−3534.
(43) Loge, R. E.; Suo, Z. Nonequilibrium Thermodynamics of Ferroelectric Domain Evolution. *Acta Mater.* **1996**, *44*, 3429−3438.
(44) Merz, W. J. Double Hysteresis Loop of $BaTiO_3$ at the Curie Point. *Phys. Rev.* **1953**, *91*, 513−517.
(45) Schultz, A. M.; Zhang, Y.; Salvador, P. A.; Rohrer, G. S. Effect of Crystal and Domain Orientation on the Visible-Light Photochemical Reduction of Ag on $BiFeO_3$. *ACS Appl. Mater. Interfaces* **2011**, *3*, 1562−1567.
(46) Wenderich, K.; Mul, G. Methods, Mechanism, and Applications of Photodeposition in Photocatalysis: A Review. *Chem. Rev.* **2016**, *116*, 14587−14619.
(47) Jones, P. M.; Dunn, S. Interaction of Stern Layer and Domain Structure on Photochemistry of Lead-Zirconate-Titanate. *J. Phys. D: Appl. Phys.* **2009**, *42*, No. 065408.
(48) Kalinin, S. V.; Bonnell, D. A.; Alvarez, T.; Lei, X.; Hu, Z.; Ferris, J. H.; Zhang, Q.; Dunn, S. Atomic Polarization and Local Reactivity on Ferroelectric Surfaces: A New Route toward Complex Nanostructures. *Nano Lett.* **2002**, *2*, 589−593.
(49) Burbure, N. V.; Salvador, P. A.; Rohrer, G. S. Photochemical Reactivity of Titania Films on $BaTiO_3$ Substrates: Origin of Spatial Selectivity. *Chem. Mater.* **2010**, *22*, 5823−5830.
(50) Wang, X.; Xu, Q.; Li, M.; Shen, S.; Wang, X.; Wang, Y.; Feng, Z.; Shi, J.; Han, H.; Li, C. Photocatalytic Overall Water Splitting Promoted by an α-β Phase Junction on Ga_2O_3. *Angew. Chem.* **2012**, *124*, 13266−13269.

DOI: 10.1021/acsami.8b16983
ACS Appl. Mater. Interfaces 2018, 10, 41450−41457

Supporting Information

Influence of the Magnitude of Ferroelectric Domain Polarization on the Photochemical Reactivity of $BaTiO_3$

Wenjia Song, Paul A. Salvador, and Gregory S. Rohrer∗

Department of Materials Science and Engineering, Carnegie Mellon University,

Pittsburgh, Pennsylvania 15213, United States

∗Corresponding author.

E-mail address: gr20@andrew.cmu.edu (G.S. Rohrer).

EBSD data processing

The EBSD patterns were then indexed by the TSL orientation imaging microscopy (OIM) software using the high temperature cubic structure as the reference frame. (The room temperature crystal structure of $BaTiO_3$ is tetragonal, but the a/c ratio is close to 1.[1] Therefore, while it is challenging for the EBSD system to distinguish the <100> directions from the [001] direction in the tetragonal structure, indexing in the cubic structure is straightforward). The data was then processed using the following procedures to minimize the artifacts without altering the results. First, all data points with a confidence index lower than 0.1 were removed from the map and their pixels were colored black. Second, a grain dilation operation was applied with a tolerance angle of 5° and a minimum grain size of 10 pixels (grains were also required to contain multiple rows of pixels). This dilation changed the orientations of only 6 % of the pixels. Finally, an average orientation was assigned to each grain, again using a 5° tolerance angle.

Figure S1 shows an inverse pole figure map of the $BaTiO_3$ surface, where each color represents one distinguishable orientation in the standard stereographic triangle, as defined by the inset legend. The orientation (surface normal vector) of the grain labeled "L" is 6.1° from <001>. The orientation of the grain labeled "R" is 6.3° from <001>. The designations R and L will be used to refer to these grains in the main text.

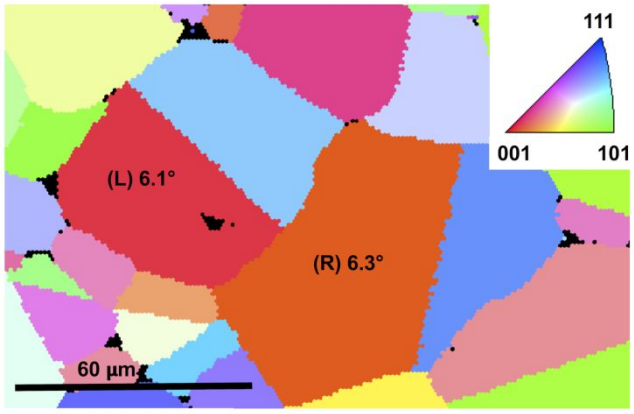

Figure S1. Inverse pole figure map of the polycrystalline $BaTiO_3$ surface. The orientation associated with each color is defined by the inset legend, showing the standard stereographic triangle for cubic crystals. The left (L) and right (R) grains have orientations 6.1° and 6.3° from <001>, respectively.

To explore the domain structure evolution over time in a quenched $BaTiO_3$ sample, photoreduction of silver was conducted on the same surface. By comparing the deposit pattern

right after quenching (as shown in Figure S2a and S2c) and 13 days after (as shown in Figure S2b and S2d), it can be observed that the domain structure evolved; most of the 180° domain walls disappeared.

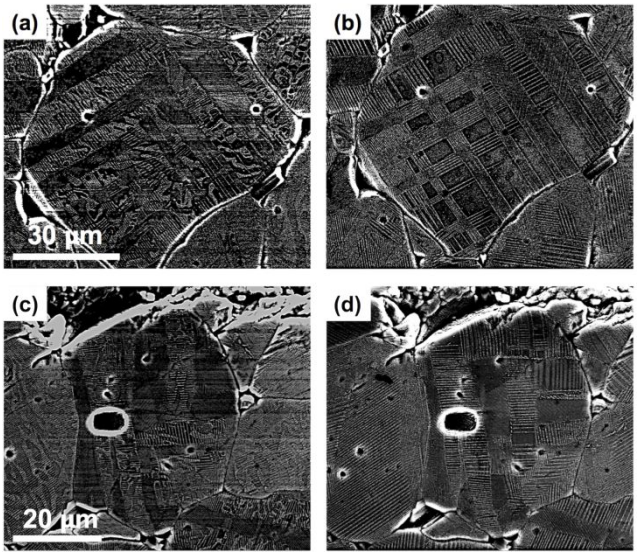

Figure S2. (a) and (c) Secondary electron image on a BaTiO3 surface with an orientation close to {001} after the photochemical reaction in aqueous silver nitrate solution. The sample was annealed and quenched in DI water at room temperature before the reaction. The surface was cleaned and the same silver photoreduction reaction was repeated after 13 days. The secondary electron image of the same area is shown in (b) and (d).

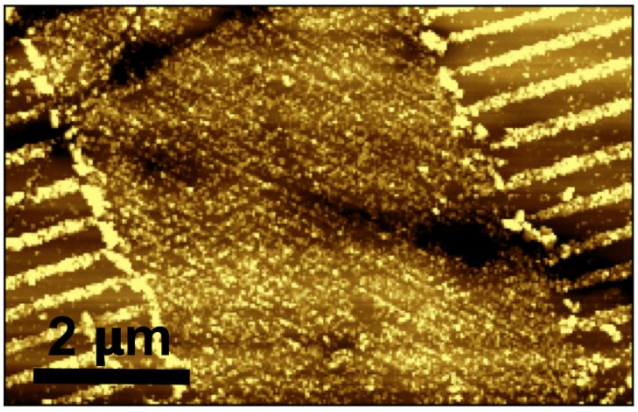

Figure S3. An enlarged image of the left bottom part of Figure 1a. The topographic contrast is 35 nm from black to white.

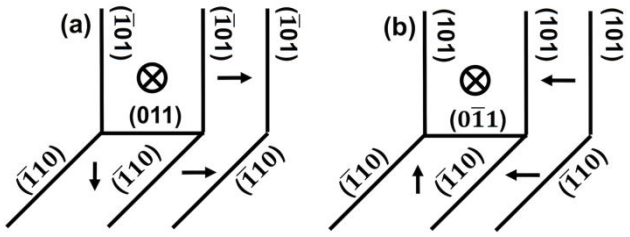

Figure S4. (a) and (b) The schematics showing the two possible polarizations and the corresponding domain wall orientations on a (001) grain surface, modified from Figure 5b and 5e to explain the possible 45° stripes of weak reactivity between the ladders in Figure 1a.

References

(1) Uchino, K.; Sadanaga, E.; Hirose, T. Dependence of the Crystal Structure on Particle Size in Barium Titanate. *J. Am. Ceram. Soc.* **1989**, *72*, 1555–1558.